Available online at www.sciencedirect.com
SCIENCE DIRECT®
Journal of Nuclear Materials 327 (2004) 211–219
journal of nuclear materials
www.elsevier.com/locate/jnucmat

Development of a master sintering curve for ThO_2

T.R.G. Kutty [a,*], K.B. Khan [a], P.V. Hegde [a], J. Banerjee [a], A.K. Sengupta [a], S. Majumdar [a], H.S. Kamath [b]

[a] *Radiometallurgy Division, Bhabha Atomic Research Centre, Trombay, Mumbai 400 085, India*
[b] *Nuclear Fuels Group, Bhabha Atomic Research Centre, Trombay, Mumbai 400 085, India*

Received 7 January 2003; accepted 16 February 2004

Abstract

A master sintering curve for ThO_2 containing 0.5 wt% CaO has been constructed with the help of combined-stage sintering model. The concept of the master sintering curve (MSC) has been used to calculate the activation energy for sintering for the above composition, and a value of 520 kJ/mol was obtained. The validity of MSC has been verified by the data of a few experimental runs using a high temperature dilatometer. With one temperature dependent parameter determined experimentally (Θ), it became possible to describe accurately the densification behavior of ThO_2 from the early to final stages of sintering. The sinterability of powder compacts made from different powders and fabrication procedures under different thermal histories, could be characterized through the master sintering curve.

PACS: 81.20.Ev; 61.72.−y; 66.30.Fq

1. Introduction

ThO_2 pellets are usually fabricated by the conventional powder metallurgy technique. Large-scale production of these pellets is carried out by the process consisting of cold compaction followed by high temperature sintering in reducing atmosphere at around 1650 °C. The powder is first compacted to cylindrically shaped green pellets which contain about 40–50% of porosity. This is followed by high temperature sintering, during which most of the porosities are eliminated and the pellet attains a density greater than 95% of its theoretical density. An important processing goal for the nuclear ceramics is to obtain the uniform microstructure with the desired grain size. It is also important to attain the desired dimension after sintering since the tolerance on the pellet diameter is small. The oversized pellets are to be ground to the desired size and the undersized pellets are to be reprocessed. It is therefore desirable to predict the final size and density of the pellets. In the conventional sintering procedure, the parameters such as time and temperature of the sintering are arbitrarily decided on the 'trial and error' basis. It could be beneficial for the nuclear industry to predict the densification behavior from the sintering data that are readily available. If the prediction is made, the sintering strategy could be established on that basis [1], which leads to produce the pellets of good quality with less number of rejects. Therefore, there is a need for better understanding of whole sintering procedure. The theory of master sintering curve (MSC) provides a new insight into the understanding of sintering [2–5].

The master sintering curve enables to predict the densification behavior under arbitrary time–temperature excursions with the help of a minimum of preliminary experiments. This curve is sensitive to such factors as starting morphology of the powder, fabrication route, dominant diffusion mechanism and heating condition used for sintering [6]. Thus, it requires a different MSC if

* Corresponding author. Tel.: +91-22 559 2466; fax: +91-22 550 5151.
E-mail address: tkutty@magnum.barc.ernet.in (T.R.G. Kutty).

0022-3115/$ - see front matter
doi:10.1016/j.jnucmat.2004.02.007

any of the above-mentioned factors are changed before it is used to predict sintering behavior. The MSC curve can also be used as an aid to compare the sinterability of different powders and to know the effects of additives, atmosphere and fabrication procedure of sintering. This concept has been extended recently into the pressure regime, so the final density at any applied pressure can be predicted [1]. The master sintering curve has been successfully applied to several sintering systems such as Al_2O_3, ZnO, $Al_2O_3 + 5\%ZrO_2$, $Al_2O_3 + 5\%TiO_2$, rhenium and nickel powders [1,6].

2. Theory

The master sintering curve can be derived from the densification rate equation of the combined-stage sintering model. The underlying principle of the combined-stage sintering model is briefly described below [7–11]:

2.1. Combined-stage sintering model

The sintering is caused by heat treatment of porous specimen without or with the application of external pressure, in which some properties of the pellet are changed with the reduction of the surface energy to those of the pore-free system. The sintering of a powder compact is traditionally divided into three stages in which different mechanisms may be operative [12–24]. They are

- initial stage sintering, where the neck forms and grows between individual particles,
- intermediate stage sintering, where the neck growth results in continuous networks of tubular pores,
- final stage sintering, where the continuity of pore channels is broken into individual pores which are located at the grain boundaries or inside the grains.

Most of the sintering models focus on a specific idealized geometry that is represented by only one of the three stages in the above sintering process. This leads the following problems, viz. [7]:

(a) This approach does not allow the consideration of entire sintering process from beginning to end.
(b) The idealized geometry must be assumed in order to calculate diffusional flows analytically.

To overcome the above-mentioned drawback, it is desirable to have a model that describes the entire sintering process. The combined-stage sintering model, proposed by Hansen et al. [7], describes the densification through the entire stages of sintering. By observing the similarities in the three stages of sintering, a single equation was derived which describes the densification through all stages of sintering. Johnson and Su [2] showed that the observed sintering rates in the combined-stage sintering model were within the range expected for the diffusion controlled sintering at the heating rates used. In this model the microstructure is characterized by two separate parameters representing geometry and the average grain size. In general, however, the starting microstructure and the evolution of the microstructure of actual powder compacts during the sintering is quite different from those described by any of the sintering models. As a result, the sintering kinetics of the most system cannot be predicted quantitatively by the existing models [8]. Therefore, the challenge encountered in developing combined-stage sintering model is to find a method for correctly quantifying the complex stages in microstructure, which occur during the sintering.

2.2. Master sintering curve

As mentioned earlier, the master sintering curve can be derived from the densification rate equation of the combined-stage sintering model [6]. For the development of master sintering curves, the parameters in the sintering rate equations are separated into (a) those related to the microstructure and (b) those related to time and temperature terms, on the opposite sides of the equation [1]. These two sides are then related to each other experimentally.

The combined-stage sintering model relates the linear shrinkage rate of a compact at any given instant to the grain boundary and volume diffusion coefficients, the surface tension and certain aspects of the instantaneous microstructure of the compact. In this model, the instantaneous linear shrinkage rate is given as [8]:

$$-\mathrm{d}L/L\,\mathrm{d}t = (\gamma\Omega/kT)[(\Gamma_{\mathrm{v}}D_{\mathrm{v}}/G^3) + (\Gamma_{\mathrm{b}}\delta D_{\mathrm{b}}/G^4)], \qquad (1)$$

where $\mathrm{d}L/L\,\mathrm{d}t$ is the normalized instantaneous linear shrinkage rate, γ is the surface energy, Ω the atomic volume, k the Boltzmann constant, T the absolute temperature, G the mean grain diameter, D_{v} and D_{b} the coefficients of volume and grain boundary diffusion respectively, δ the width of the grain boundary, Γ_{v} and Γ_{b} are the collections of microstructure scaling parameters for volume and grain boundary diffusion respectively.

For isotropic shrinkage, the linear shrinkage rate can be converted into the densification rate by

$$-\mathrm{d}L/L\,\mathrm{d}t = \mathrm{d}\rho/3\rho\,\mathrm{d}t, \qquad (2)$$

where ρ is the bulk density.

Substituting Eq. (2) in (1) and assuming that only one of the diffusion mechanisms (either volume or grain boundary diffusion) dominates the sintering process, we can rewrite Eq. (1) as [6]:

$$\mathrm{d}\rho/3\rho\,\mathrm{d}t = (\gamma\Omega/kT)\Gamma_{(\rho)}D_0/(G_{(\rho)})^n \exp(-Q/RT), \quad (3)$$

where Q is the activation energy and D_0 is the pre-exponential factor. R is the gas constant.

The above equation can be rearranged and integrated as follows:

$$\int_{\rho_0}^{\rho} (G_{(\rho)})^n/(3\rho\Gamma_{(\rho)})\mathrm{d}\rho = \int_0^t (\gamma\Omega D_0)/(kT) \times \exp(-Q/RT)\,\mathrm{d}t. \quad (4)$$

In the above equation, the atomic diffusion process and the microstructural evolution terms are separated [1]. All the terms on the right hand side (rhs) of Eq. (4) are related to atomic diffusion process and are independent of characteristics of powder compacts. The terms on the left hand side (lhs) are the quantities that define the microstructural evolution and are independent of the thermal history of the powder compacts [6].

The time and temperature dependent side (rhs) of the equation can be represented as theta parameter, Θ, as follows [1]:

$$\Theta = \int_0^t 1/T \exp(-Q/RT)\,\mathrm{d}t, \quad (5)$$

where t is the instantaneous time, which is usually a function of temperature. Similarly one could integrate the lhs of Eq. (4) if the evolution of the microstructure is known in detail.

Eq. (5) can be simplified for isothermal portion of the sintering runs to [1]:

$$\Theta = t_i/T \exp(-Q/RT), \quad (6)$$

where t_i is the duration of the isothermal portion of the run. For constant heating rate, Eq. (5) can be written as:

$$\Theta = (1/c)\int_{T_0}^{T} 1/T \exp(-Q/RT)\,\mathrm{d}T, \quad (7)$$

where c is the heating rate used and T_0 is the temperature below which no sintering takes place.

The relationship between the density (ρ) and Θ is defined as the master sintering curve. For the construction of MSC, a series of runs at different temperatures (isothermal) or constant heating rates over a range of heating rates is needed. If the activation energy of sintering is unknown, it has to be estimated in order to obtain the master sintering curve.

3. Construction of MSC

For the construction of MSC, the integral of Eq. (5) and the experimental density should be known. The dilatometry can be conveniently used to determine the density since the instantaneous density at all times can be obtained from the dilatometric data [25]. For the calculation of Θ, the activation energy for the sintering process must be known. If the activation energy is unknown, it can be estimated with good precision from Θ versus density (ρ) data [1,6]. For this purpose, a particular value of activation energy is chosen and ρ–Θ curves are constructed for each heating rate. If the curves fail to converge, a new value of activation energy is chosen and the calculations are repeated. This procedure should be continued until all the curves are converged showing that the activation energy is the acceptable one for sintering [1]. A curve can be then fitted through all the data points, and then convergence of data to the fitted line can be quantified through the sum of residual squares of the points with respect to the fitted line. The best estimate of Q will be the value of the minimum in the plot of activation energy versus mean residual squares [6].

3.1. Limitations of MSC

Several assumptions are made in developing the above MSC which are listed below [1]:

1. The microstructural evolution is dependent only on density for any given powder and the fabrication procedure.
2. One of the diffusion mechanisms either volume or grain boundary diffusion dominate the sintering process.
3. Contributions from surface diffusion and vapor transport are negligible in the sintering process.
4. This procedure should be applied only to the powder compacts made from the same source powder and the same fabrication procedure.

With this background, we will discuss about the experimental procedure carried out using a high temperature dilatometer for the generation of a master sintering curve for ThO_2.

4. Experimental

4.1. Fabrication of green pellet

The green ThO_2 pellets for this study were prepared by the conventional powder metallurgy technique which consists of the following steps:

- milling of the as-received thorium oxide powder in a planetary ball for 8 h using tungsten carbide balls to break its platelet morphology,
- mixing/milling of the above milled ThO_2 powder with the required quantity of additive (0.5 wt% CaO) for 4 h in the planetary ball mill with tungsten carbide balls,

- double precompaction at 150 MPa for 5 s,
- granulation of the precompacts,
- final cold compaction of the granulated powder at 300 MPa using a dwell time of 5 s into green pellets.

To facilitate compaction and to impart handling strength to the green pellets, 1 wt% zinc behenate was added as lubricant/binder and mixed during the last 1 h of the mixing/milling procedure. The green pellets were 8.15 mm in diameter and around 8 mm in length. The green density of ThO_2 pellets was about 68%. The characteristics of the pure ThO_2 powder used in this study are given in Table 1.

4.2. Dilatometry

The shrinkage of ThO_2 was measured with a push rod type dilatometer in axial direction. The length change measurements were made by a linear voltage differential transducer (LVDT) which was maintained at a constant temperature by means of water circulation from a constant temperature bath. The accuracy of the measurement of change in length was within ±0.1 μm. The temperature was measured using a calibrated thermocouple which is placed directly above the sample. A small force of 0.2 N was applied to the sample through the push rod. The heating rate used for the above studies was 3, 12 and 30 K/min. Up to 200 °C, all the pellets used for dilatometric experiments were heated using a heating rate of 10 K/min to drive out moisture and volatile impurities. The expansion of a standard sample (POCO graphite, NIST) was measured under identical conditions in order to give correction for the expansion of the system. Table 2 gives the typical impurity contents of a sintered pellet.

The dilatometric experiments were carried out in Ar–8%H_2 atmosphere using a flow rate of 18 l/h. Length measurement was made in situ under dynamic condition. As the sample is heated, its temperature and length values were measured continuously with the help of a thermocouple and LVDT, respectively.

The precise lattice parameter of the ThO_2 containing 0.5 wt% CaO pellet after sintering was determined from the high angle X-ray diffraction scan and was found to be 5.5954 Å. As per Vegard's law, the lattice parameter of ThO_2 containing 0.5 wt% CaO should be 5.5789 Å. But the experimentally determined value of lattice parameter (5.5954 Å) is higher than the calculated value using Vegard's law. The deviation from Vegard's law may be explained as follows.

The addition CaO to ThO_2 creates defects since calcium has a lower valency than thorium. ThO_2 is always stoichiometric unless deviations from stoichiometry are produced chemically, e.g., by adding CaO to produce oxygen deficient $(Th,Ca)O_{2-x}$. Such materials produce one oxygen vacancy per added impurity atom due to the charge neutrality condition. It has been reported that the variation of lattice parameter with composition can be accounted for by the relative size of the ions [26]. In case of compound like Pu(C,O), when carbon atom is replaced by oxygen atom of smaller size, the lattice parameter of Pu(C,O) has been found decreasing [27]. In ThO_2–CaO solid solution, Th^{4+} ion of radius 0.99 Å is replaced by a bigger Ca^{2+} ion of radius 1.06 Å [28]. When a smaller Th^{4+} ion is replaced by a bigger Ca^{2+} ion, the lattice parameter of ThO_2–CaO solid solution will increase. However due to the creation of anionic vacancies, lattice parameter of the above will slightly decrease. Since relative ionic size effect is more dominant, the resultant lattice parameter will be higher than that calculated using Vegard's law. Also it is probable that solid solution formation between ThO_2 and CaO may be incomplete. On account of the above, ThO_2–CaO solid solution will not follow the Vegard's law.

The theoretical density of the solid solution has been calculated using the experimentally determined values of lattice parameter and was found to be 9.83 g/cm^3.

Table 1
Characteristics of pure ThO_2 powder (before the addition of CaO)

Property	Value
Oxygen to metal ratio	2.00
Apparent density (g/cm^3)	0.70
Total impurities (ppm by wt)	<1200
Theoretical density, ρ (g/cm^3)	10.00
Specific surface area, S (m^2/g)	1.53

Table 2
Impurities in the sintered ThO_2 pellet containing 0.5 wt% CaO

Element	Impurity (ppm by wt)
Na	17
Al	6
Mg	4
Si	<100
Fe	9
Cr	<1
Co	<5
Ni	<1
Mo	<5
W	<50
Cu	1.5
B	<0.6

5. Results

Fig. 1 shows the dL/L_0 versus temperature plot of ThO_2 under different heating rates in Ar–8%H_2 atmosphere. It can be seen from the figure that the onset of

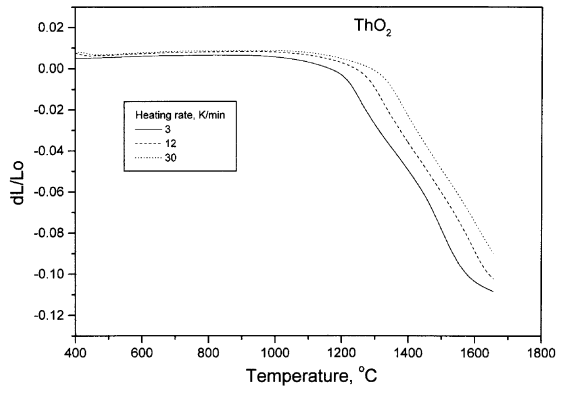

Fig. 1. Shrinkage curves for ThO_2 pellets containing 0.5 wt% CaO as dopant in Ar–8%H_2 atmosphere for the different heating rates. The dL/L_0 values are plotted against temperature, where L_0 is the initial length.

shrinkage is shifted to higher temperatures on increasing the heating rates. The dilatometric curves of Fig. 1 were replotted as percentage of theoretical density (%TD) versus temperature (Fig. 2). The dL/L_0 values were converted into %TD using the following relation [25]:

$$\rho = [1/(1 - dL/L_0)]^3 \rho_0, \tag{8}$$

where ρ and ρ_0 are the densities of the sintered and green pellets, respectively. The curves have the familiar sigmoidal shape and generally shifted to higher temperatures with increasing heating rate. It can be noted that the sintered densities obtained at any temperature showed a modest but a systematic dependence on heating rate. The density was found to increase at 1300 °C approaching a maximum value greater than 90% of TD

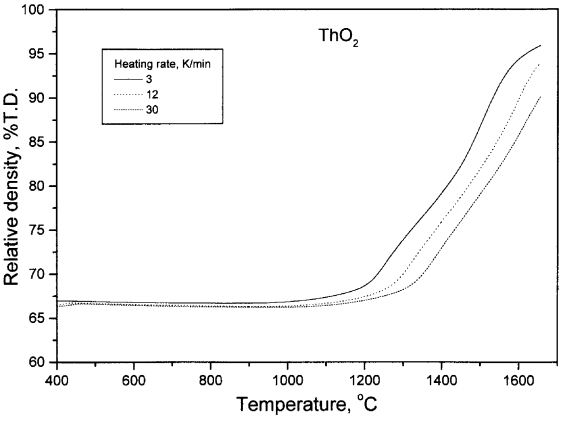

Fig. 2. Shrinkage curves of Fig. 1 are replotted as percent of theoretical density (%TD) versus temperature for CaO doped ThO_2 pellets. The dL/L_0 values were converted into % TD using relation (8).

The maximum density was found to depend upon the heating rate, the higher the heating rate the lower the sintered density.

As mentioned earlier, one of the essential data for obtaining the master sintering curve is the activation energy. For this, the density data for ThO_2 obtained from the dilatometric measurements, and Θ values obtained from Eq. (5) are employed. A ρ–Θ curve is then constructed for all the heating profiles for a chosen value of activation energy (350 kJ/mol) as shown in Fig. 3(a). It can be seen that the curves for different heating rates are not converging. Now a new value of activation energy is chosen and the calculation is repeated. The curves at 500, 600 and 750 kJ/mol are shown in Fig. 3(b)–(d), respectively. The best convergence occurs at around 550 kJ/mol. Fig. 4 gives the mean residual squares for the various values of activation energy and the minimum has been found to be for 520 kJ/mol. The activation energy thus obtained was found to be in reasonable agreement with the values reported in the literature [29–32]. Matzke [29,31] reported 650 kJ/mol for pure ThO_2. According to Shiba [33], it is 625 kJ/mol. The activation energy obtained in this study is about 20% less than the value obtained by Matzke. The difference may be because the sample used in this study contains about 0.5 wt% CaO as sintering aid.

The activation energy for densification is a characteristic quantity that elucidates the fundamental diffusion mechanisms during the sintering process. Traditionally, it has been obtained from the shrinkage rate from either isothermal heating or constant heating rate experiments. The present result indicates that an alternate method exists on the basis of MSC for the determination of the activation energy of sintering if it is unknown [1].

From the knowledge of the activation energy of sintering, MSC for ThO_2 has been constructed and is shown in Fig. 5. It can be seen that the value of Θ changed dramatically from 10^{-50} at the beginning to 10^{-35} at the higher density end. Despite a 10-fold rise in heating rate, the individual sintering curves have merged reasonably close to a single curve. This result suggests that there must be a general curve, regardless of sintering path, which is what we have defined as the MSC [6].

6. Validation of master sintering curve

Before applying MSC to the industrial practice, MSC has to be validated with a sufficient amount of data. For this the following experiments were carried out:

These experiments were carried out in a dilatometer using Ar–8%H_2 as the cover gas. For this, three pellets of ThO_2 + 0.5 wt% CaO composition were compacted under identical condition as described in Section 4.1. These green pellets were used for the above study using

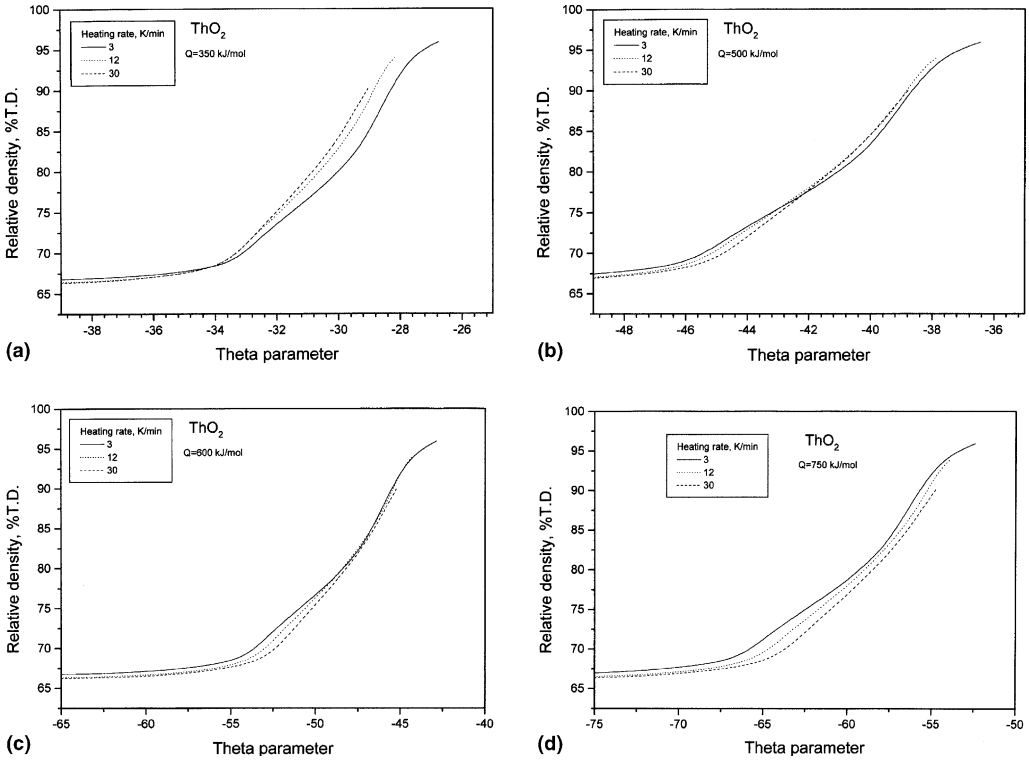

Fig. 3. Estimation of activation energy from the master sintering curve. Construction of a ρ–Θ curve for the different heating profiles for a chosen value of activation energy: (a) 350 kJ/mol, (b) 500 kJ/mol, (c) 600 kJ/mol, (d) 750 kJ/mol.

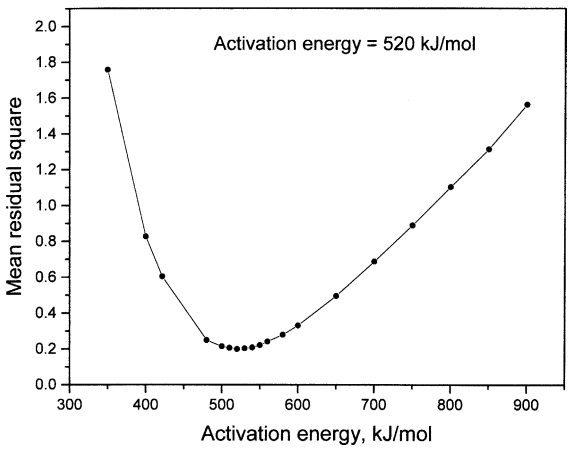

Fig. 4. Mean residual squares for the various values of the activation energy.

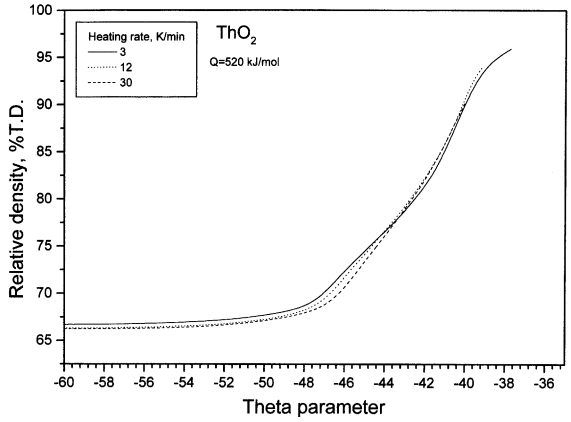

Fig. 5. Master sintering curve for 0.5%CaO doped ThO_2. The curve is constructed using an activation energy of 520 kJ/mol.

the dilatometer. Up to 200 °C, the pellet was heated using a slow heating rate of 10 K/min to drive out moisture and other volatile impurities. For further heating, a heating rate of 20 K/min was used. The first pellet was held at 200 °C for 20 min in order to drive out all volatile impurities. Then the above pellet was sintered by heating up to 1300 °C and isothermally holding at that temperature for 3 h. The soak at 200 °C is given only to the sample that was heated to 1300 °C. Since the dilatometric curve did not show any deviation or slope change, we did not opt this soak for the other two samples. The second and third pellet was sintered in dilatometer at 1400 °C for 4 h and 1500 °C for 2 h,

respectively. The sintered density of the above-mentioned pellets was measured geometrically. It was found to be 78%, 83.5% and 91% of theoretical density (TD) for the pellets sintered at 1300 °C/3 h, 1400 °C/4 h and 1500 °C/2 h, respectively (Table 3).

Fig. 6 shows the shrinkage versus isothermal hold time for the pellets sintered at 1300 °C/3 h, 1400 °C/4 h and 1500 °C/2 h. In this plot, abscissa represents the total time, i.e., the time required to reach the temperature as well as the isothermal hold on time. From the dilatometric data of a particular run, the Θ values are calculated for constant heating regime using the relation given in Eq. (7) and that for the isothermal hold using Eq. (6). These values are shown on the master sintering curve as shown in Fig. 7. It can be seen that the values for all the three temperatures with different periods of time are lying on the MSC, validating the concept of MSC. For clarity only a few representative data points are shown. But the trend is very clearly brought out. Thus it can be regarded that integration of a proposed sintering time–temperature profile yields a point on the MSC curve. The expected density can be obtained by finding the ordinate value at that point. On the other hand, if the final desired density is known, it is possible to find out the corresponding Θ value from the abscissa of the master sintering curve and thereafter to plan the sintering schedule [34–36]. Thus MSC can be a characteristic measure of the sinterability of a powder compact over a wide range of density.

Table 3
Typical values of green and sintered densities of ThO_2 pellets doped with 0.5% CaO

Sintering schedule		Density (%TD)	
Temperature (°C)	Time (h)	Green density	Sintered density
1300	3	68	78
1400	4	68	83.5
1500	2	68	91

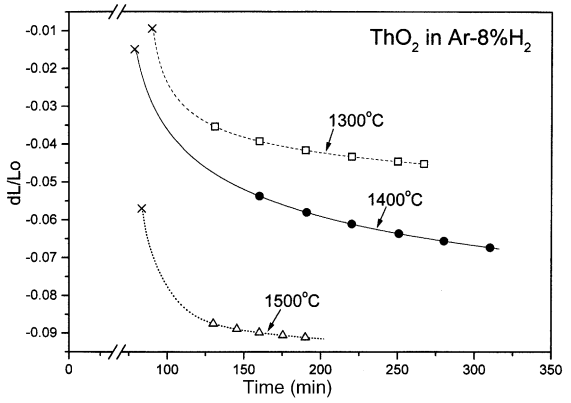

Fig. 6. The shrinkage curves for 0.5%CaO doped ThO_2 pellets in Ar–8%H_2 atmosphere during the isothermal heating for various periods of time at 1300, 1400 and 1500 °C. The time shown is the total time including the time required to reach the particular temperature.

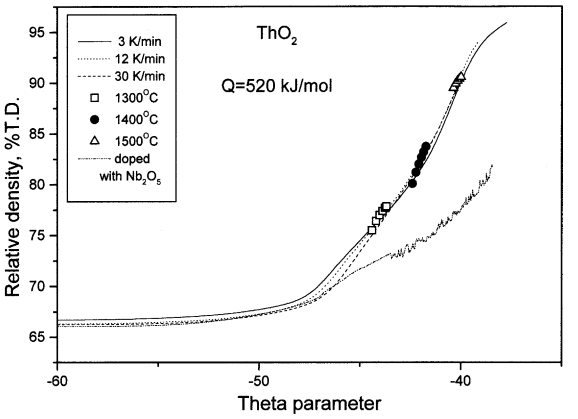

Fig. 7. Validation of master sintering curve for 0.5%CaO doped ThO_2. The experimental values for three temperatures are shown. The master sintering curve developed for 0.25%Nb_2O_5 doped ThO_2 is also shown.

In the second set of experiment, the effect of dopant on MSC has been evaluated. To study this, ThO_2 pellets were fabricated under the identical condition with Nb_2O_5 as dopant instead of CaO. The shrinkage behavior of this pellet has been measured using the dilatometer under the identical condition that was used for $ThO_2 + 0.5$ wt% CaO. From the shrinkage data, the density values were calculated using Eq. (8). The master sintering curve for the above composition was constructed as per the procedure laid down in Section 5, which was shown together in Fig. 7. This curve does not coincide with that of ThO_2 doped with CaO. This result clearly shows that MSC is dependent on dopant. In other words, the sinterability of powder compacts made from different powders, dopants and fabrication procedures could be characterized with the help of the master sintering curve. The master sintering curve for ThO_2 doped with Nb_2O_5 showed oscillations. This may be due to the following reason. When one Th^{4+} ion is substituted by one Nb^{5+} ion in the ThO_2 lattice, the effective positive charge of +1 is imparted on the lattice. Hence the addition of Nb_2O_5 to ThO_2 causes to form significantly high concentrations of oxygen interstitial ions. However, in the reducing atmosphere like Ar–8%H_2, Nb_2O_5 is also reduced to lower oxides: $Nb_2O_5 \rightarrow NbO_2 \rightarrow Nb_2O_3 \rightarrow NbO$. This means that niobium acts as a lower valency additive to ThO_2 in a reducing atmosphere. The oscillation in the shrinkage curves as well as in the MSC may be due the reduction of Nb_2O_5 to the lower oxides.

As mentioned earlier in Section 3.1, we have made many assumptions on developing the master sintering curve for ThO_2. Let us examine the validity of these assumptions on the basis of the present study. It was assumed that the microstructural evolution is dependent only on density. The sintering experiments carried out on both metals of Cu and Ni powders, and ceramics such as Al_2O_3, BeO and ZnO have proved that the average grain size is dependent only on density and is independent of the sintering temperature and the heating rate employed [8,10,37,38]. Coble and Gupta [39] have shown that the mechanism for grain growth and densification is the same with the same activation energy. Similar results have been reported by Allen et al. [40] from their study on neutron scattering and also by Chen and Mayo [41] from their study on ZrO_2. Experiments conducted on Ni and Al_2O_3 [6,8] powders have demonstrated that the Γ parameters of Eq. (1) are functions of only density. On the basis of the above observation on some common ceramics and metals, it may be expected that ThO_2 should behave in a similar way.

It was also assumed that either of the diffusion mechanisms (volume or grain boundary) dominates in the sintering process. The volume diffusion tends to dominate at high temperatures and for compacts with large sized powders, while the grain boundary diffusion dominates in the sintering process with small particle size at lower temperatures. Since sintering of ThO_2 has been carried out at high temperatures ($>0.4T_m$), the volume diffusion is expected to play the major role in diffusion related processes. Also, the study carried out by the authors, on the sintering kinetics of UO_2–50%PuO_2 [42] and PuO_2 [43] pellets, showed that the mechanism for the initial stages of sintering was volume diffusion. The other assumptions to neglect the vapor transport and surface diffusion are also legitimate in our case since the vapor transport takes place only at very high temperatures or in corrosive atmospheres and the surface diffusion is usually predominant at low temperatures below $0.3T_m$. Since we have not used any corrosive atmosphere and the temperature of sintering was below 1700 °C, the contribution from vapor transport will be negligible. In short, the assumptions used for developing the master sintering curve for ThO_2 have been found to be appropriate.

7. Conclusions

The master sintering curve provides a useful tool to quantify the densification behavior of a given powder compact. In this study, the curve for ThO_2 containing 0.5 wt% CaO has been constructed with the help of combined-stage sintering model. The following conclusions were drawn:

1. The concept of MSC has been used to calculate the activation energy for sintering for the above composition.
2. The activation energy for sintering for ThO_2 containing 0.5 wt% CaO was found to be 520 kJ/mol.
3. The validity of MSC has been verified by a few experimental runs using a dilatometer.
4. With one experimentally determined temperature dependent parameter (Θ), the densification behavior for ThO_2 can be described from the early to the final stages of sintering.
5. The sinterability of powder compacts made from different powders and fabrication procedures under different thermal histories, could be characterized through the master sintering curve.

References

[1] D.L. Johnson, H. Su, Ceram. Bull. 76 (2) (1997) 72.
[2] D.L. Johnson, H. Su, in: Proceedings of 1997 International Conference on Powder Metallurgy and Particulate Materials, Part 14, 1997, p. 115.
[3] D.L. Johnson, M. Henrichsen, J. Hwang, V.P. Dravid, J. Am. Ceram. Soc. 83 (11) (2000) 2861.
[4] M. Stocker, Auto Technol. 2 (2002) 38.
[5] Northwestern News (Ed.), Chris Chandler, 24/6/1996, Northwestern University, 1996.
[6] H. Su, D.L. Johnson, J. Am. Ceram. Soc. 79 (12) (1996) 3211.
[7] J.D. Hansen, R.P. Rusin, M. Teng, D.L. Johnson, J. Am. Ceram. Soc. 75 (5) (1992) 1129.
[8] H. Su, D.L. Johnson, J. Am. Ceram. Soc. 79 (12) (1996) 3199.
[9] F. Parhami, R.M. McMeeking, A.C.F. Cocks, Z. Suo, Mech. Mater. 31 (1999) 43.
[10] M. Chu, M.N. Rahaman, L.C. De Jonghe, R.J. Brook, J. Am. Ceram. Soc. 74 (6) (1991) 1217.
[11] D.L. Johnson, M.H. Teng, L.D. Marks, J. Mater. Res. 12 (1) (1997) 235.
[12] D.R. Olander, Fundamental aspects of nuclear reactor fuel elements, TID- 26711-P1, US Department of Energy, 1976, p. 145.
[13] F. Thummler, W. Thomma, Metall. Rev. 115 (1967) 69.
[14] R.L. Coble, J.E. Burke, in: J.E. Burke (Ed.), Progress in Ceramic Science, Vol. 3, Pergamon, Oxford, 1963, p. 197.
[15] M. Mayo, Int. Mater. Rev. 41 (3) (1996) 85.
[16] H. Palmour, D.R. Johnson, in: G.C. Kuczynski, N.A. Hooton, C.F. Gibbs (Eds.), Sintering and Related Phenomena, Gordon and Breach, New York, 1967, p. 779.
[17] G.C. Kuczynski, Trans. Am. Inst. Mining Met. Eng. 185 (2) (1949) 169.
[18] R.L. Coble, J. Appl. Phys. 32 (5) (1961) 787.
[19] D.L. Johnson, T.M. Clarke, Acta Met. 12 (1964) 1173.
[20] R.L. Coble, J. Am. Ceram. Soc. 41 (1958) 55.
[21] D.L. Johnson, I.B. Cutler, J. Am. Ceram. Soc. 46 (1963) 541.
[22] W.D. Kingery, M. Berg, J. Appl. Phys. 26 (1955) 1205.

[23] L. Berrin, D.L. Johnson, in: G.C. Kuczynski, N.A. Hooton, C.F. Gibbs (Eds.), Sintering and Related Phenomena, Gordon and Breach, New York, 1967, p. 369.
[24] D.L. Johnson, J. Appl. Phys. 40 (1969) 192.
[25] T.R.G. Kutty, P.V. Hegde, K.B. Khan, S.N. Pillai, A.K. Sengupta, G.C. Jain, S. Majumdar, H.S. Kamath, D.S.C. Purushotham, J. Nucl. Mater. 305 (2002) 159.
[26] E.C. Subbarao, P.H. Sutter, J. Hrizo, J. Am. Ceram. Soc. 48 (9) (1965) 443.
[27] G.C. Jain, C. Ganguly, J. Nucl. Mater. 207 (1993) 169.
[28] J. Emsley, The Elements, 3rd Ed., Clarendon, Oxford, 1998, p. 48, 210.
[29] Hj. Matzke, J. Chem. Soc., Faraday Trans. 86 (1990) 1243.
[30] C.R.A. Catlow, in: T. Sorensen (Ed.), Non-stoichiometric Oxides, Academic, New York, 1981, p. 61.
[31] Hj. Matzke, J. Nucl. Mater. 114 (1983) 121.
[32] J.L. Wolfrey, M.J. Bannister, J. Am. Ceram. Soc. 55 (8) (1972) 390.
[33] K. Shiba, in: R.P. Ararwala (Ed.), Diffusion Processes in Nuclear Materials, North Holland, Amsterdam, 1992, p. 71.
[34] D.L. Johnson, D. Sohn, Cement Concr. Res. 29 (2) (1999) 241.
[35] D.L. Johnson, J.J. Host, M.H. Teng, B.R. Elliott, J.-H. Hwang, T.O. Mason, J.R. Weertman, V.P. Dravid, J. Mater. Res. 12 (5) (1997) 1268.
[36] D.L. Johnson, J.-H. Hwang, V.P. Dravid, M.H. Teng, J.J. Host, B.E. Elliott, J.R. Weertman, T.O. Mason, J. Mater. Res. 12 (4) (1997) 1076.
[37] J. Wang, R. Raj, J. Am. Ceram. Soc. 73 (5) (1990) 1170.
[38] T.K. Gupta, J. Am. Ceram. Soc. 55 (5) (1972) 276.
[39] R.L. Coble, T.K. Gupta, in: G.C. Kuczynski, N.A. Hooton, C.F. Gibbs (Eds.), Sintering and Related Phenomena, Gordon and Breach, New York, 1967, p. 423.
[40] A.J. Allen, G.G. Long, S. Krueger, in: 97th Annual Meeting of American Ceramic Society, Cincinnati, OH, Paper no. SXV-29-95, 3 May 1995.
[41] D.J. Chen, M.J. Mayo, J. Am. Ceram. Soc. 79 (4) (1996) 906.
[42] T.R.G. Kutty, P.V. Hegde, R. Keswani, K.B. Khan, S. Majumdar, D.S.C. Purushotham, J. Nucl. Mater. 264 (1999) 10.
[43] T.R.G. Kutty, K.B. Khan, P.V. Hegde, A.K. Sengupta, S. Majumdar, D.S.C. Purushotham, J. Nucl. Mater. 297 (2001) 120.